

Single and double photoemission and generalizations

Y. Pavlyukh^{1,*}

¹*Institut für Physik, Martin-Luther-Universität Halle-Wittenberg, 06120 Halle, Germany*

A unified diagrammatic treatment single and double electron photoemission currents is presented. The lesser density-density response function is the starting point of these derivations. Diagrams for higher order processes in which several electrons are observed in coincidence can likewise be obtained. For physically relevant situations in which the photoemission cross-section can be written as the Fermi Golden rule, the diagrams from the nonequilibrium Green's function approach can be put direct correspondence with that of the scattering theory.

PACS numbers: 71.10.-w, 31.15.A-, 73.22.Dj

I. INTRODUCTION

The electron photoemission is a process in which classical or quantized electromagnetic field interacts with a many-body target leaving the system in an unbound electronic state [1]. This subclass of optical absorption processes can further be categorized according to the number of emitted particles in one scattering event, i.e., single, double or, more generally, n -electron photoemission. The exact quantum state the ionized target was left in is typically not known. However, since detectors can determine the asymptotic scattering state of emitted electrons some information about the ionized target can be inferred by virtue of energy and momentum conservation laws. In particular, one can tell whether the target was left in the ground or an excited state. Thus, we can distinguish between the no-loss photoelectron current and that incorporating losses. The processes leading to the emission of an electron with a reduced energy can have various origins. On the basis of the empirical three step model [2] we have a picture where a liberated electron propagates through the sample losing its energy on the way. In this way the electron-photon interaction and the inelastic electron scattering are considered as two independent processes and for the latter one speaks about the *extrinsic* energy losses [3, 4]. Besides electronic excitations the phonon [5], impurity scattering [6] and Auger processes [7, 8] are important.

On the other hand electron-electron interaction in the system causes the spectral function (or the density of states) to deviate from the non-interacting one in which all spectral weight is confined to a quasiparticle peak. A typical picture would be a quasiparticle peak followed by a sequence of satellite peaks. Their origin can be different as well [9–11]. For instance in the photoemission from a deep core level it is the density oscillations in the system — plasmons — that form scattering channels responsible for the occurrence of plasmonic satellites. S -model proposed by Lundqvist [12] and solved by Langreth [13] captures exactly this effect and predicts a sequence equally spaced satellite peaks with oscillator strengths satisfying the Poisson distribution. If an electron originates from one of such peaks it will come to a detector with a reduced energy. One speaks here about the *intrinsic* energy losses be-

cause it is the ground state spectral density that is modified by the plasmon scattering [14, 15].

Although first microscopic theories of photoemission [16, 17] have taken underlying electronic structure into account they have not provided a description of inelastic energy losses experienced by the liberated electron. Such formulation was achieved with the help of non-equilibrium Green's function approach by Caroli *et al.* [18]. The starting point of their treatment is the zeroth order triangular diagram where two vertices are situated on the forward and backward tracks of the Keldysh contour [19] and describe the light-matter interaction, whereas the third vertex lying at the common point of the two tracks in the remote future describes the detector state. There are no interaction lines because the photoemission is possible even for non-interacting systems. Each electron-photon interaction vertex is associated with the minimal coupling part of the Hamiltonian and is linearly proportional to the field amplitude. The whole diagram, as expected, is quadratic in the field strength and is linearly proportional to the intensity or to the number of absorbed photons.

Progressing diagrammatically further [20] one realizes that dressing of this diagram leads not only to the renormalization of each electronic propagator involved, but also generates vertex functions [21]. All these ingredients are important in different physical scenarios, they account for the effects of optical field screening [22–24], intrinsic and extrinsic losses as well as their interference [25–27], and for the formation of the scattering states [28]. The goal of this work is to give a diagrammatic description of the multiparticle emission. Before proceeding with corresponding diagrammatic construction a short account of the single photoemission will be given in Sec. II. Properties of double photoemission diagrams are discussed in Sec. III and generalization to n -particle emission is presented in Sec. IV. The formalism looks more natural if irreducible density-density response function describing general photoabsorption process is used as a starting point. Such point of view has already been mentioned by Feibelman and Eastman [29] in their derivation of the Fermi Golden rule (FGR) expression for photoemission starting with the diagrammatic approach of Caroli *et al.* [18]. Supported by work on positive definite diagrammatic approximations [21, 30, 31] a one-to-one correspondence between the NEGF (provided they can be written in the Fermi Golden rule form) and Goldstone diagrams in scattering theory [32–34] can be established as is outlined here.

* yaroslav.pavlyukh@physik.uni-halle.de

In this work atomic units are used throughout.

II. INGREDIENTS OF SPE

The differential cross-section fully describes the photoemission experiment. It relates the electron current $J_{\mathbf{k}}$ to the incoming photon flux density F :

$$\frac{d\sigma}{d\mathbf{k}} = \frac{J_{\mathbf{k}}}{F}$$

The incident photon flux is obtained by dividing the incident intensity $I = \frac{\omega^2 A^2}{2\pi c}$ by the photon energy ω . The current is determined by the electronic structure of the system and by details of its coupling to the electromagnetic field, in velocity gauge we have $\hat{\Delta} = \frac{1}{c}\mathbf{A} \cdot \hat{\mathbf{p}}$, where $\hat{\mathbf{p}}$ is the momentum operator. Many-body perturbation theory yields diagrammatic expansion of the current [16, 18, 20, 21, 24, 35] in terms of Green's functions on the Keldysh contour [19]. It results in

$$J_{\mathbf{k}} = \lim_{\eta \rightarrow 0} 2\eta \int_{-\infty}^0 d(tt') e^{\eta(t+t')} (\Delta^* \mathbf{Z}^{(1)}(t, t') \Delta)_{\mathbf{k}}, \quad (1)$$

with the following ground state correlator

$$Z^{(1)}(t, t') = \langle \Psi_0 | c_b^\dagger(t) c_a(t) c_{\mathbf{k}}^\dagger(0) c_{\mathbf{k}}(0) c_c^\dagger(t') c_d(t') | \Psi_0 \rangle, \quad (2)$$

where the field operators are in the Heisenberg representation. Three parts can be seen: operators dependent on the times $t, t' \in (-\infty, 0]$ originate from the light-matter couplings $\hat{\Delta}^\dagger(t) = \sum_{ab} \Delta_{ba}^* c_b^\dagger(t) c_a(t)$ and $\hat{\Delta}(t') = \sum_{cd} \Delta_{cd} c_c^\dagger(t') c_d(t')$, whereas $c_{\mathbf{k}}^\dagger(0) c_{\mathbf{k}}(0)$ yields the current operator. This is the reason why $Z^{(1)}(t, t')$ is sometimes called the *three-current* correlator. The system interacts with electromagnetic field in the interval of time from remote past to the moment $t = 0$ where the observation takes place. This entails the specific time-order of the operators in the correlator and is the reason why the standard time-order formalism is insufficient for its computation (no Kubo formula for photoemission [17]). On the other hand the time-ordering in (2) can naturally be represented on the Keldysh contour, Fig. 1(a). The correlator can be perturbatively computed by applying the Wick's theorem.

Specification of the single-particle indices for the creation and annihilation operators in Eq. (2) is important. The unbound (continuum) states are denoted in bold-style to distinguish them from general indices denoted as a, b, c, \dots that also comprise bound states i, j, k, \dots . In zeroth order there is a single diagram resulting from the following contraction

$$\langle c_b^\dagger(t_+) c_a(t_+) c_{\mathbf{p}}^\dagger(0) c_{\mathbf{p}}(0) c_c^\dagger(t'_-) c_d(t'_-) \rangle.$$

Other contractions vanish because the target is bound in its ground state, i.e.

$$c_{\mathbf{k}} | \Psi_0 \rangle = 0. \quad (3)$$

Introducing the *lesser* and *greater* Green's function (GF) components

$$G_{ab}^<(t_1, t_2) \equiv G_{ab}^{+-}(t_1, t_2) = i \langle c_b^\dagger(t_2) c_a(t_1) \rangle, \quad (4a)$$

$$G_{ab}^>(t_1, t_2) \equiv G_{ab}^{-+}(t_1, t_2) = -i \langle c_a(t_1) c_b^\dagger(t_2) \rangle. \quad (4b)$$

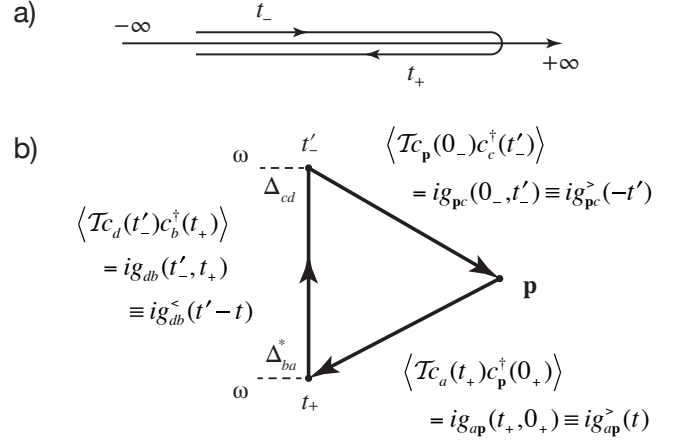


FIG. 1. (a) The Keldysh time-loop contour C . The forward branch is denoted with a “+” label while the backward branch is denoted by a “-” label. (b) Lowest order diagram for single photoemission. $\hat{\Delta}$ is the operator for light-matter coupling associated with vertices having time arguments t'_- and t_+ .

condition (3) can be formulated as the requirement that lesser GFs with one or more continuum indices vanish:

$$G_{ka}^< = G_{ak}^< = 0.$$

In these notations zeroth order (in Coulomb interaction v) correlator is given by the product of one lesser GF describing the propagation of an added hole and two greater GFs describing propagation of the emitted particle [see Fig. 1(b)]:

$$Z^{(1)}(t, t') = ig_{ap}^>(t) g_{db}^<(t' - t) g_{pc}^>(-t'). \quad (5)$$

The constituent GFs are mean-field ones, i.e. they are averages over the ground state of corresponding Hartree-Fock Hamiltonian (we assume that it is bound and fulfills a condition similar to (3)). The vertical electron propagator, i.e., the one that connects two electron-photon vertices, is of the *lesser* kind $G^< \equiv G^{-+}$ because its first and second time arguments belong to different tracks, “-” and “+” respectively. It contains the information on the spectral density of the occupied states. Replacing the bare with the full propagator means that mean-field spectral density of occupied states is replaced with the exact interacting one which also incorporates the intrinsic energy losses. Computation of the correlated spectral densities is the main goal of electronic structure theory. The electronic lines flowing to or from the detector are of the *greater* type and, thus, are associated with unoccupied electronic states. Their dressing describes the formation of *scattering* states observed in the detector [28, 36, 37].

In addition to renormalization of fermionic lines the evaluation of next orders of Eq. (2) leads to appearance of vertex functions. As Almladh explains [21, 22] they amount to modification of the bare light-matter coupling operator $\hat{\Delta}$ by the vector-coupling vertex function $\hat{\Lambda}(\epsilon + \omega, \epsilon)$. All other possible renormalizations of $Z^{(1)}(t, t')$ contain renormalized interaction lines connecting points on the forward and backward branches of the contour and are associated with extrinsic en-

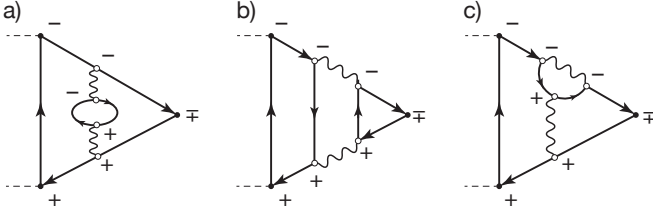


FIG. 2. Lowest order diagrams with extrinsic losses. Wavy lines denote the bare Coulomb interaction. Pluses and minuses indicate to which branch of the Keldysh contour [Fig. 1(a)] corresponding points are belonging.

ergy losses. In the next section we consider a particular example of such processes involving emission of a secondary electron.

III. DOUBLE PHOTOEMISSION

There are several possibilities to introduce double photoemission. One way is to regard it as a single photoemission process accompanied by extrinsic energy losses whereby a liberated electron interacts with the target system knocking out a secondary electron. In atomic, molecular and optical (AMO) physics community [34, 38] this is known as the *knock out* mechanism. As an illustration consider second order diagrams at Fig. 2. They are discussed in details by Caroli *et al.* as examples of extrinsic losses (cf. Fig. 9 of Ref. [18]). There are no first order processes because bare Coulomb interaction is local in time and, therefore, cannot connect points on different branches of Keldysh contour. In all three cases there is a fermionic line flowing from “-” to “+” vertex, i.e., given by the greater GF. This is a potential candidate for a secondary electron that can be detected in the coincidence measurement. Intuitively corresponding DPE diagrams can be drawn by cutting this line and adding an intermediate point with well defined momentum \mathbf{p}_2 . These and several more diagrams describing double photoemission can be obtained applying the Wick theorem to the following correlator [35]:

$$Z^{(2)}(t, t') = \langle \Psi_0 | c_b^\dagger(t) c_a(t) c_{\mathbf{k}_1}^\dagger(0) c_{\mathbf{k}_2}^\dagger(0) \times c_{\mathbf{k}_2}(0) c_{\mathbf{k}_1}(0) c_c^\dagger(t') c_d(t') | \Psi_0 \rangle. \quad (6)$$

The derivation is simpler if this correlator is written in the real space representation. For completeness all leading order (second order in bare Coulomb interaction) diagrams are shown on Fig. 3, where points labelled by α, β, γ denote integration over space, summation over spin, and integration over the time on “-”-branch of the Keldysh contour. Similarly, χ, ν, ζ correspond to the points on the “+”-branch. Specifically, $\alpha \equiv (\mathbf{x}_\alpha, t_\alpha) \equiv (\mathbf{r}_\alpha, \sigma_\alpha, t_\alpha)$, $\chi \equiv (\mathbf{x}_\chi, t_\chi) \equiv (\mathbf{r}_\chi, \sigma_\chi, t_\chi)$, etc. Let us recall explicit form of the non-interacting greater GF:

$$g_{\mathbf{x}_\alpha \mathbf{x}_\zeta}^>(t, t') = -i \sum_a \bar{f}(\epsilon_a) e^{-i\epsilon_a(t-t')} \langle \mathbf{x}_\alpha | a \rangle \langle a | \mathbf{x}_\zeta \rangle, \quad (7)$$

where $f(\epsilon) = 1 - \bar{f}(\epsilon)$ is the zero temperature Fermi distribution function and the sum runs over all one-particle states.

For times $t, t' \in (-\infty, 0]$ the product of two greater GFs can be expressed as:

$$\begin{aligned} & \sum_y g_{\mathbf{x}_\alpha y}^>(t, 0) g_{y \mathbf{x}_\zeta}^>(0, t') \\ &= (-i)^2 \sum_{ab} \bar{f}(\epsilon_a) \bar{f}(\epsilon_b) e^{-i\epsilon_a t + i\epsilon_b t'} \sum_y \langle \mathbf{x}_\alpha | a \rangle \langle a | y \rangle \langle y | b \rangle \langle b | \mathbf{x}_\zeta \rangle \\ &= (-i)^2 \sum_a e^{-i\epsilon_a(t-t')} \bar{f}(\epsilon_a) \langle \mathbf{x}_\alpha | a \rangle \langle a | \mathbf{x}_\zeta \rangle \\ &= -i g_{\mathbf{x}_\alpha \mathbf{x}_\zeta}^>(t, t'), \end{aligned} \quad (8)$$

where the completeness of the one-particle basis was used. The sum over y can be done as integration over space coordinates and spin indices or in any other complete basis. For instance we can perform the sum in the basis of single-particle states, i.e. $\sum_y \rightarrow \sum_i + \sum_{\mathbf{k}}$, where i labels bound states and \mathbf{k} is the continuum state labeled by its momentum. Cutting a greater non-interacting GF amounts to specification of an intermediate state, e.g. $g_{\mathbf{x}_\alpha \mathbf{x}_\zeta}^>(t, t') \rightarrow g_{\mathbf{x}_\alpha \mathbf{k}}^>(t, 0) g_{\mathbf{k} \mathbf{x}_\zeta}^>(0, t')$. To the left hand side we see a single GF that describes the propagation of an electron. Its intermediate state is not determined, whereas the product of two GFs at the right hand side describes observation of the intermediate state in the detector. This procedure can be used to generate double photoemission diagrams starting from that of single photoemission accompanied by energy losses. Considering diagrams on Fig. 2 we see that they in particular transform into the diagrams 4A, 4A', and 4C, respectively, as shown on Fig. 3. This figure contains a number of other topologically distinct species which can be obtained by considering in addition to extrinsic losses, the diagrams describing intrinsic losses, and interference of these two mechanisms. The outlined procedure can be generalized to obtain SPE diagrams from that of the density-density response function $\chi^<(t, t')$, DPE from SPE, and so on:

$$Z_{\mathbf{k}}^{(1)}(t, t') = \int d(\alpha \zeta) \frac{\delta \chi^<(t, t')}{\delta g_{\mathbf{x}_\alpha \mathbf{x}_\zeta}^>(\tau_\alpha, \tau_\zeta)} g_{\mathbf{x}_\alpha \mathbf{k}}^>(\tau_\alpha, 0) g_{\mathbf{k} \mathbf{x}_\zeta}^>(0, \tau_\zeta), \quad (9a)$$

$$Z_{\mathbf{k} \mathbf{k}'}^{(2)}(t, t') = \int d(\gamma \nu) \frac{\delta Z_{\mathbf{k}}^{(1)}(t, t')}{\delta g_{\mathbf{x}_\gamma \mathbf{x}_\nu}^>(\tau_\gamma, \tau_\nu)} g_{\mathbf{x}_\alpha \mathbf{k}'}^>(\tau_\gamma, 0) g_{\mathbf{k} \mathbf{x}_\zeta}^>(0, \tau_\nu). \quad (9b)$$

In this way the 4C-type diagram is a descendant of the SPE diagram in Fig. 4(b) which, in turn, traces back to the density-density response function in Fig. 4(a).

It is more than just graphs operations that is illustrated here. In ref. [39] and in a sequence of works [30, 31] it has been shown that cutting procedure, which splits diagrams representing the lesser or the greater response function into *half-diagrams*, can be used to construct approximations with the positive definiteness property. These are the approximations for response functions possessing positive spectral functions in the whole frequency range. Explicit construction outlined there shows that in this case the spectral function can be written in the FGR form, that is, as a sum of terms containing squared modulus of the matrix element of a certain scattering process multiplied with corresponding δ -function assuring overall energy conservation. The matrix element then is

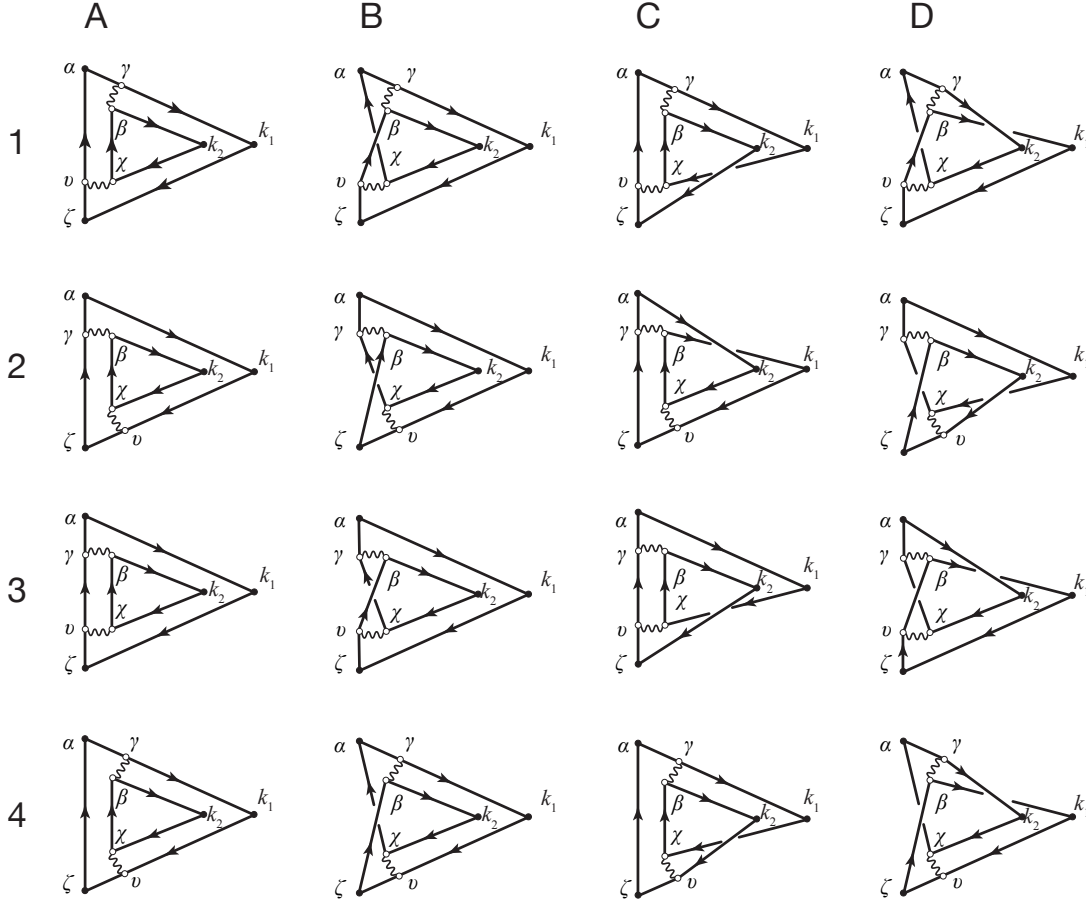


FIG. 3. Leading order diagrams describing double photoemission. Notation 1A, 1B, etc., is used. Exchange of \mathbf{k}_1 and \mathbf{k}_2 generates topologically new ones. Corresponding columns will be denoted as A', B', and so on.

expressed in terms of GFs on only one branch of the Keldysh contour, i. e. all its vertices are labeled with either “+” or with “-”.

For scattering problems as considered here the Fermi Golden rule approach is particularly useful. It allows to describe arbitrary scattering processes in leading order without referring to complicated mathematical apparatus of Feynman diagrams. It is also the only choice for more complicated processes if perturbative expressions cannot readily be gen-

erated. Therefore, it is interesting to identify the ingredients of diagrams on Fig. 3, i. e., the half-diagrams yielding corresponding expressions in the FGR form. Independently whether the second-order density-density response diagrams (many of them are listed by Uimonen *et al.* [31]) are used as a starting point, or the single photoemission diagrams listed for instance by Caroli *et al.* [18], or the one shown here on Fig. 3, the result will be topologically identical. The difference is in the treatment of dangling lines: in the former case their quantum numbers are summed over, whereas in SPE one dangling line is observed in the detector and therefore has a fixed index. For emission of n -particles by one photon there should be n dangling lines corresponding to momenta registered (in coincidence) in the detectors. Rather surprisingly, the result of such analysis (Fig. 5) is quite simple and can be recovered from early works of Amusia and Kazachkov [38], they can also be identified as diagrams in Fig. 7(b) in Uimonen *et al.* [31]. In order to make explicit parallels with works of AMO physics community consider Goldstone diagrams (see Chang and McDowell [40] for a short summary of this technique in application to atomic photoionization and L’Huillier *et al.* [41] for more complicated multiphoton examples) that are commonly used in scattering theory. To make this work

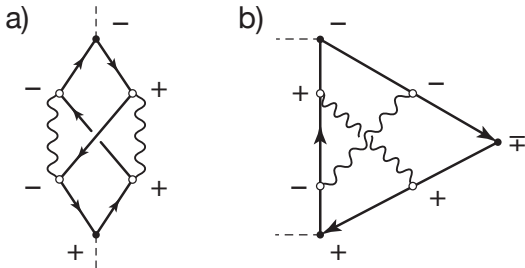


FIG. 4. Application of cutting procedure to the lesser density-density response function (left) yields a SPE diagram (right) which, in turn, leads to the 4C-type diagram shown on Fig. 3.

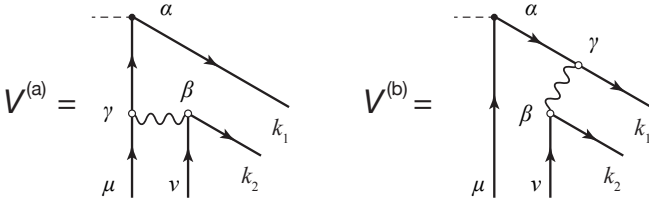


FIG. 5. Half-diagrams corresponding to Fig. 3. Same labeling is preserved. All vertices have time arguments on “-”-branch of the Keldysh contour. $V^{(a)}$ has interaction line connected to the lesser propagator for primary electron, the scattering reflects intrinsic losses in the ground state. In AMO physics this process is also known as *shake off* mechanism. In contrast, $V^{(b)}$ has interaction line connected to the greater propagator for primary electron, the scattering reflects extrinsic losses in excited state. In AMO physics this process is also known as *knock out* mechanism. There two more topologically equivalent structures with exchanged \mathbf{k}_1 and \mathbf{k}_2 indices. They will be denoted as $\bar{V}^{(a)}$ and $\bar{V}^{(b)}$.

self-contained corresponding lowest order DPE Goldstone diagrams are shown in Fig. 6 (cf. Fig. 8.1 in ref. [34]).

In fact, Goldstone diagrams carry more information than standard NEGF ones: the direction of arrow on each fermionic line specifies whether particle or hole propagator should be used. For the latter, “+” and “-” assigned to the vertices only specify the branch of Keldysh contour they belong to; however, all possible mutual ordering within the branch have to be considered. That is why there are twice as many diagrams in Fig. 6 as compared to Fig. 5: the two possibilities correspond to the two terms in the time-ordered GF of internal line.

Let us verify that all triangular DPE diagrams at Fig. 3 can be obtained by gluing half-diagrams in Fig. 5. The simplest identities would be

$$Z^A = \sum_{\mu\nu} |V^{(a)} + V^{(b)}|_{\mu\nu}^2,$$

$$Z^{A'} = \sum_{\mu\nu} |\bar{V}^{(a)} + \bar{V}^{(b)}|_{\mu\nu}^2,$$

where Z^A denotes the sum of contributions from column “A”

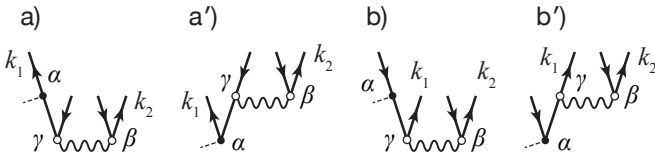


FIG. 6. Goldstone diagrams corresponding to the matrix elements of double photoemission in Fig. 5. For NEGF diagrams + and - assigned to the vertices partly determine the time ordering; here, the direction of arrows specifies whether particle (arrow up) or hole (arrow down) propagators should be used. Therefore, each scattering matrix element shown in Fig. 5 is represented by two diagrams: $V^{(a)}$ by (a) and (a'), $V^{(b)}$ by (b) and (b'). This reflects the fact that in addition to dangling lines which are described by either particle or hole propagators, $V^{(a)}$ and $V^{(b)}$ contain one internal g^{--} line. It is given by time-ordered propagator comprising both the particle and the hole terms.

of Fig. 3, the indices μ and ν label dangling lines, and momentum dependence, i. e. $\mathbf{k}_{1,2}$, is not shown explicitly. This is not the full set because, as explained in refs. [30, 31] permutations of dangling lines must also be considered:

$$Z^B = \sum_{\mu\nu} (V^{(a)} + V^{(b)})_{\mu\nu} (V^{(a)} + V^{(b)})_{\nu\mu}^*.$$

Collecting all contributions the full set at Fig. 3, i. e. $Z^{(2)} = Z^A + Z^{A'} + Z^B + Z^{B'} + Z^C + Z^{C'} + Z^D + Z^{D'}$ can be obtained as follows:

$$Z^{(2)} = \sum_{\mu\nu} (V + \bar{V})_{\mu\nu} (V + V^T + \bar{V} + \bar{V}^T)_{\mu\nu}^*, \quad (10)$$

where the sum of diagrams in Fig. 5 is denoted by $V = V^{(a)} + V^{(b)}$. There are 32 terms in this expression. The construction guarantees the positivity of corresponding two-particle current.

IV. GENERALIZATIONS

This construction can be generalized to the process of emission of arbitrary number of particles. It is clear that higher order diagrams need to be considered. Already an example of classical system of particles with two-body hard sphere interactions shows that emission of n particles requires at least $n - 1$ collisions. Quite generally, in order to achieve n -particle emission Goldstone diagrams must contain at least $n - 1$ interaction lines, the scattering cross-section is being proportional to $v^{2(n-1)}$ as shown in ref. [35]. However, what can be said about topological structure of these diagrams?

One possibility to characterize diagrammatic complexity is to enumerate possible topological structures. For equilibrium many-body perturbation theory the problem of counting diagrams was initiated in the work of Molinari [42] who suggested to use the Hedin's system of functional equations [43, 44] that relates the electron GF, the proper self-energy Σ , vertex function Γ , polarization P , and the effective potential W as the generating functions for corresponding diagram counting. The transformation from integral-functional equations to much simpler differential equations for generating functions is done by collapsing all space, spin and time coordinates into one point, i. e., considering zero-dimensional case. These equations have been subsequently solved analytically [45]. Besides pure mathematical interest, the solution can be used as a basis for method development [46, 47] and to get insight into the convergence of approximate theories [48, 49].

We have seen above that arbitrary photoemission process can be described using the lesser density-density response function ($\chi^<$) as a starting point. Corresponding time-ordered irreducible response (P^{--}) is the polarization in Hedin's system of equations [44]. Thus, it seems natural to use the nonequilibrium extension of these equations [50, 51] in order to enumerate *decorated* Feynman diagrams (with “+” and “-” assigned to the vertices). Below, these equations are explicitly written discarding the time and space dependence of

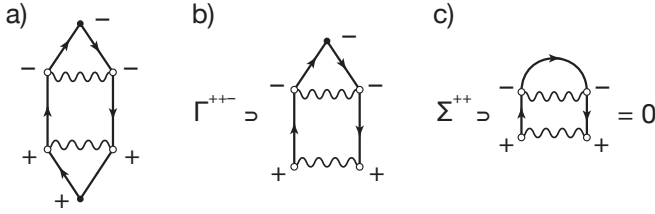


FIG. 7. (a) Example of polarization that cannot be obtained from Eq. (11b). Corresponding vertex function (b) can be constructed by applying Eq. (11c) to self-energy (c).

all quantities (in zero dimensions), but preserving the labeling of vertices:

$$\Sigma^{\eta\bar{\eta}} = i \sum_{\eta_3 \eta_4} \bar{\eta}_3 \bar{\eta}_4 W^{\eta\eta_3} G^{\eta\eta_4} \Gamma^{\eta_4 \bar{\eta}_3 \eta}, \quad (11a)$$

$$P^{\eta\bar{\eta}} = -i \sum_{\eta_3 \eta_4} \bar{\eta}_3 \bar{\eta}_4 G^{\eta\eta_3} G^{\eta_4 \eta} \Gamma^{\eta_3 \eta_4 \bar{\eta}}, \quad (11b)$$

$$\Gamma^{\eta_1 \eta_2 \eta_3} = \delta_{\eta_1 \eta_2} \delta_{\eta_2 \eta_3} + g^{\eta_4 \eta_3} g^{\eta_3 \eta_5} \frac{\delta \Sigma^{\eta_1 \eta_2}}{\delta g^{\eta_4 \eta_5}}, \quad (11c)$$

$$G^{\eta\bar{\eta}} = g^{\eta\bar{\eta}} + g^{\eta\bar{\eta}} \Sigma^{\eta\bar{\eta}} G^{\eta\bar{\eta}} - g^{\eta\eta} \Sigma^{\eta\bar{\eta}} G^{\eta\bar{\eta}} + g^{\eta\eta} \Sigma^{\eta\eta} G^{\eta\bar{\eta}}, \quad (11d)$$

$$W^{\eta\bar{\eta}} = v P^{\eta\eta} W^{\eta\bar{\eta}} - v P^{\eta\bar{\eta}} W^{\eta\bar{\eta}}. \quad (11e)$$

Here $\eta = \pm 1$ denotes branches of Keldysh contour, $\bar{\eta} = -\eta$. In equations for the screened interaction some terms are not present because the bare interaction is instantaneous, i.e. $v^{\eta\bar{\eta}} = 0$. One more assumption was incorporated: in Dyson's equations for GFs it was explicitly used that in equilibrium (or in steady state) and at zero temperature the following convolutions vanish $\int d\bar{t} X^{\eta\bar{\eta}}(t, \bar{t}) Y^{\eta\bar{\eta}}(\bar{t}, t') = 0$ (see discussion by Ness *et al.* [51]). Under this assumption equations for time-ordered and anti-time-ordered functions are reduced to the usual form. From the structure of equations (11) the vertices are necessarily decorated such that no isolated islands of pluses or minuses appear [30, 31].

Let us now skip $\pm i$ prefactors and signs (not essential for the diagram enumeration), introduce the prefactor ℓ into eq. (11b) in order to keep count of fermionic loops and write the power series solution for $P^<$:

$$\begin{aligned} P^{<} &= 3\ell v g^{<} g^{<} \{[g^{<}]^2 + [g^{>}]^2\} \\ &+ v^2 g^{<} g^{<} \{(5\ell^2 + 15\ell)([g^{<}]^4 + [g^{>}]^4) \\ &+ 6\ell[g^{<}]^2[g^{>}]^2 + (8\ell^2 + 8\ell)g^{<} g^{<} g^{<} g^{>}\} \\ &+ O(v^3). \end{aligned}$$

The $(8\ell^2 + 8\ell)$ term numbers all diagrams in Fig. 3, however, three other terms of the second order (they contain a single greater propagator and therefore contribute only to SPE, but

not to DPE) are missing $[3\ell v^2 g^{<} g^{<} [g^{<}]^2 [g^{>}]^2]$; one such example is shown in Fig. 7(a)]. This can be traced back [Fig. 7(c)] to the self-energy $\Sigma^{\eta\eta}$ in the vertex equation (11c). Per construction (recall that we impose $X^{\eta\bar{\eta}} Y^{\eta\bar{\eta}} = 0$) it contains only $g^{\eta\eta}$ lines and is therefore insufficient to obtain the vertex function shown in Fig. 7(b). Thus, a mere extension of Hedin's equations to nonequilibrium case does not allow to enumerate photoemission diagrams. Spurious diagrams appear if restriction $X^{\eta\bar{\eta}} Y^{\eta\bar{\eta}} = 0$ is lifted, otherwise valid diagrams are missing. There is, actually, a logical explanation to this fact: due to asymmetric position of the vertex function the Hedin's expressions for the self-energy and polarization do not respect the FGR form pertinent to exact $\Sigma^{\eta\bar{\eta}}$ and $P^{\eta\bar{\eta}}$.

V. CONCLUSIONS

In this work the NEGF diagrams for single- and multi-electron emission were treated consistently by using the lesser density-density response ($\chi^<$) as a common generating function. In this way n -particle emission is described by diagrams containing n lesser electron propagators with a well defined momentum. Alternatively, the photoemission cross-section can be recasted in the Fermi Golden rule form. It is common to write corresponding matrix elements in terms of Goldstone diagrams. Gluing such diagrams relating to the time-propagation in forward, backward directions yields the NEGF construction. This correspondence was illustrated by considering all possible double photoemission processes to the leading order in Coulomb interaction. Equivalence between the shake off and knock out mechanisms known in AMO physics and intrinsic and extrinsic losses in condensed matter physics is demonstrated.

Since $\chi^<$ is a central quantity of this study it is desirable to have a set of functional relations that would allow to recursively generate its perturbative expansion in a manner similar to Hedin's equations for time-ordered quantities. An extension of these equations to nonequilibrium case generates a larger set of diagrams, some of them being zero at zero temperature and in a steady state. Because Hedin's equations for self-energy and polarization are not compatible with FGR these spurious diagrams cannot be easily eliminated.

ACKNOWLEDGMENTS

It is a pleasure to thank the organisers Claudio Verdozzi, Andreas Wacker and Carl-Olof Almbladh for an excellent workshop on *Progress in Nonequilibrium Green's Functions* (PNGF6). This work is supported by the DFG grants No. SFB762 and No. PA 1698/1-1.

[1] S. Hüfner, *Photoelectron spectroscopy: principles and applications*, 3rd ed., Advanced texts in physics (Springer, Berlin; New

York, 2003).

[2] C. N. Berglund and W. E. Spicer, Phys. Rev. **136**, A1030 (1964).

- [3] J.-J. Chang and D. C. Langreth, Phys. Rev. B **5**, 3512 (1972).
- [4] J.-J. Chang and D. C. Langreth, Phys. Rev. B **8**, 4638 (1973).
- [5] E. O. Kane, Phys. Rev. **147**, 335 (1966).
- [6] E. V. Chulkov, A. G. Borisov, J. P. Gauyacq, D. Sánchez-Portal, V. M. Silkin, V. P. Zhukov, and P. M. Echenique, Chem. Rev. **106**, 4160 (2006).
- [7] C. Verdozzi, P. J. Durham, R. J. Cole, and P. Weightman, Phys. Rev. B **55**, 16143 (1997).
- [8] C. Verdozzi, M. Cini, and A. Marini, Journal of Electron Spectroscopy and Related Phenomena **117-118**, 41 (2001).
- [9] F. Aryasetiawan, L. Hedin, and K. Karlsson, Phys. Rev. Lett. **77**, 2268 (1996).
- [10] Y. Pavlyukh, A. Rubio, and J. Berakdar, Phys. Rev. B **87**, 205124 (2013).
- [11] S. M. Story, J. J. Kas, F. D. Vila, M. J. Verstraete, and J. J. Rehr, Phys. Rev. B **90**, 195135 (2014).
- [12] B. I. Lundqvist, Phys. Kondens. Mater. **9**, 236 (1969).
- [13] D. C. Langreth, Phys. Rev. B **1**, 471 (1970).
- [14] D. R. Penn, Phys. Rev. Lett. **38**, 1429 (1977).
- [15] D. R. Penn, Phys. Rev. Lett. **40**, 568 (1978).
- [16] W. L. Schaich and N. W. Ashcroft, Phys. Rev. B **3**, 2452 (1971).
- [17] G. D. Mahan, Phys. Rev. B **2**, 4334 (1970).
- [18] C. Caroli, D. Lederer-Rozenblatt, B. Roulet, and D. Saint-James, Phys. Rev. B **8**, 4552 (1973).
- [19] G. Stefanucci and R. van Leeuwen, *Nonequilibrium Many-Body Theory of Quantum Systems: A Modern Introduction* (Cambridge University Press, Cambridge, 2013).
- [20] T. Fujikawa and H. Arai, Journal of Electron Spectroscopy and Related Phenomena **123**, 19 (2002).
- [21] C.-O. Almbladh, Phys. Scr. **32**, 341 (1985).
- [22] C.-O. Almbladh, Phys. Rev. B **34**, 3798 (1986).
- [23] E. E. Krasovskii, V. M. Silkin, V. U. Nazarov, P. M. Echenique, and E. V. Chulkov, Phys. Rev. B **82**, 125102 (2010).
- [24] A.-M. Uimonen, G. Stefanucci, and R. v. Leeuwen, J. Chem. Phys. **140**, 18A526 (2014).
- [25] L. Campbell, L. Hedin, J. J. Rehr, and W. Bardyszewski, Phys. Rev. B **65**, 064107 (2002).
- [26] M. Guzzo, G. Lani, F. Sottile, P. Romaniello, M. Gatti, J. J. Kas, J. J. Rehr, M. G. Silly, F. Sirotti, and L. Reining, Phys. Rev. Lett. **107**, 166401 (2011).
- [27] M. Guzzo, J. J. Kas, L. Sponza, C. Giorgetti, F. Sottile, D. Pierucci, M. G. Silly, F. Sirotti, J. J. Rehr, and L. Reining, Phys. Rev. B **89**, 085425 (2014).
- [28] L. Hedin and J. D. Lee, Journal of Electron Spectroscopy and Related Phenomena **124**, 289 (2002).
- [29] P. J. Feibelman and D. E. Eastman, Phys. Rev. B **10**, 4932 (1974).
- [30] G. Stefanucci, Y. Pavlyukh, A.-M. Uimonen, and R. van Leeuwen, Phys. Rev. B **90**, 115134 (2014).
- [31] A.-M. Uimonen, G. Stefanucci, Y. Pavlyukh, and R. van Leeuwen, Phys. Rev. B **91**, 115104 (2015).
- [32] H. P. Kelly, Phys. Rev. **136**, B896 (1964).
- [33] I. Lindgren and J. Morrison, *Atomic many-body theory*, Springer series in chemical physics No. 13 (Springer, Berlin, 1982).
- [34] M. Y. Amusia, *Atomic photoeffect*, Physics of atoms and molecules (Plenum Press, New York, 1990).
- [35] Y. Pavlyukh, M. Schüler, and J. Berakdar, Phys. Rev. B **91**, 155116 (2015).
- [36] W. Bardyszewski and L. Hedin, Phys. Scr. **32**, 439 (1985).
- [37] L. Hedin, Journal of Electron Spectroscopy and Related Phenomena **51**, 91 (1990).
- [38] M. Y. Amusia and M. P. Kazachkov, Phys. Lett. A **28**, 27 (1968).
- [39] C.-O. Almbladh, J. Phys. Conf. Ser. **35**, 127 (2006).
- [40] E. S. Chang and M. R. C. McDowell, Phys. Rev. **176**, 126 (1968).
- [41] A. L'Huillier, L. Jönsson, and G. Wendin, Phys. Rev. A **33**, 3938 (1986).
- [42] L. G. Molinari, Phys. Rev. B **71**, 113102 (2005).
- [43] L. Hedin, Phys. Rev. **139**, A796 (1965).
- [44] G. Strinati, La Rivista del Nuovo Cimento **11**, 1 (1988).
- [45] Y. Pavlyukh and W. Hübner, J. Math. Phys. **48**, 052109 (2007).
- [46] G. Lani, P. Romaniello, and L. Reining, New J. Phys. **14**, 013056 (2012).
- [47] Y. Pavlyukh, J. Berakdar, and A. Rubio, arXiv:1601.04285 [cond-mat] (2016).
- [48] J. A. Berger, P. Romaniello, F. Tandetzky, B. S. Mendoza, C. Brouder, and L. Reining, New J. Phys. **16**, 113025 (2014).
- [49] A. Stan, P. Romaniello, S. Rigamonti, L. Reining, and J. A. Berger, New J. Phys. **17**, 093045 (2015).
- [50] U. Harbola and S. Mukamel, J. Chem. Phys. **124**, 044106 (2006).
- [51] H. Ness, L. K. Dash, M. Stankovski, and R. W. Godby, Phys. Rev. B **84**, 195114 (2011).